Searching for the Overlooked: Investigating Exoplanets in SPHERE/IFS Data

Jef Libens, Max Keppens

Supervisor: Sven Kiefer

10 December 2021

Abstract

Direct imaging is een techniek om een exoplaneet rechtstreeks te kunnen visualiseren, maar wel komt met veel moeilijkheden. Om een goed resultaat te krijgen, is het nodig om reductie-technieken toe te passen om de contributie van te ster te onderdrukken. In dit verslag zijn angular differential imaging (ADI), spectral differential imaging (SDI) en de combinaties van beide methoden toegepast op 3 verschillende systemen met behulp van principal component analysis. Deze analyse biedt de mogelijkheid aan om bepaalde informatie van onze foto's af te trekken door middel van principal components. De resultaten tonen aan dat de signal to noise ratio consistent hoger is bij de combinatie van ADI en SDI dan bij een van de twee. Met de informatie over de positie van de planeet werden ook eigenschappen van de baan de exoplaneet onderzocht. Deze kwamen overeen met de literatuur, wat aanduidt dat de detectie van de planeten goed verlopen is.

Direct imaging is a technique to directly visualize an exoplanet, but this comes with difficulties. To obtain a good result, it is necessary to apply data-reduction to suppress the contribution of the star. In this research angular differential imaging (ADI), spectral differential imaging (SDI) and the combinations of both methods were applied on 3 different systems using principal component analysis. This analysis gives the opporunity to subtract certain information of our data with the use of principal components. The results show that the signal to noise ratio is consistently bigger with the combination of ADI and SDI than the methods itself. With the information of the position of the planet, properties of the orbit if the planet could me examined. These results match the values of literature, which indicates that the detection went well.

1 Introduction

In 2004, the first exoplanet was discovered by direct imaging. This was done by a team of astronomers by using the European Southern Observatory's Very Large Telescope (VLT) to produce an image of 2M1207b, an exoplanet surrounding the brown dwarf 2M1207.

After a period of 17 years, only 159 confirmed exoplanets were discovered by this direct technique of the 4893 discovered exoplanets [2]. The reason for this low number is that finding an exoplanet by direct methods brings
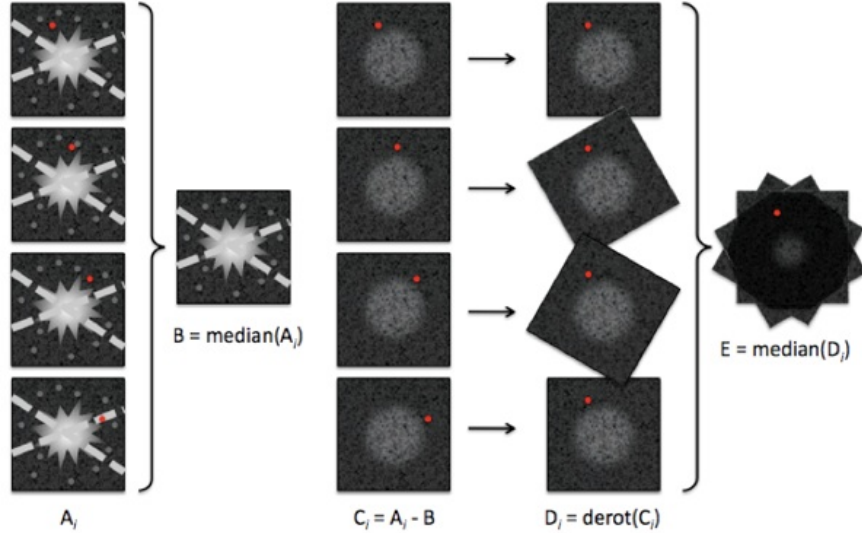
Figure 1: The steps done to perform ADI displayed schematically. First the images are made at different times, then a PCA gets done on them, not a median, as presented on the figure. The image formed by the first principal components gets subtracted from each image revealing the exoplanet. Finally the images get rotated and the median gets taken of them.

a challenge with it: exoplanets are extremely faint light sources compared to their parental star. To overcome this problem, different methods are applied to suppress the light emitted by the star. The instrument used in the VLT, namely the Spectro-Polarimetric High-contrast Exoplanet Research instrument (SPHERE), has a wavelength range of $0.95 - 1.35 \ \mu m$ and is equipped with a coronagraph to block the central region of the star to reduce its contribution to the image. In addition to this reducing method, data-reduction or imaging techniques have to be used to achieve a high contrast image where the planet is visible. The used imaging techniques in this research are called angular differential imaging (ADI) and spectral differential imaging (SDI), which will be explained in section 2.1 and 2.2. These two imaging techniques will not only be used separately, but also the combination of these methods will be applied on the data. The latter has not been done by many researchers yet, but does give overall

a better result then using ADI or SDI alone according to Kiefer et al. [3]. An important aspect of these techniques is that they use principal component analysis (see section 2.6). This analysis produces images called principal components (PC's), which are used to cut out the contribution of the star. Using different amounts of PC's will give us different processed images. In this research, these imaging methods together with machine learning techniques are implemented in an algorithm using the Python package Pynpoint. The goal is to create high contrast images of exoplanets from raw data retrieved from the ESO archive and to compare the signal to noise ratio (S/N) of images in different wavelengths and where different amounts of PC's are used. These techniques are implemented on the following three systems: HR8799, 51 Eridani and β Pictoris. The first system is chosen because this solar system has 4 known exoplanets which already have been directly imaged. The second system, 51 Eridani, only

2

has one confirmed planet: 51 Eridani b. β Pictoris has 2 confirmed exoplanets: β Pictoris b and β Pictoris c. Only the first has been directly imaged. This planet is the biggest exoplanet examined in this research. It is not expected to gain a general result which can be applied to all solar systems, because not enough solar systems are examined. The goal is to analyze these systems using different differential methods and to see how PCA can be best applied.

2 Imaging techniques

The goal of using imaging techniques is to make the planet visible by subtracting the light coming from the central star. This is necessary, because even with the state-of-the-art technology (coronagraphs, detectors, optics...) the light coming in from the planet will still be negligible compared to his parental star. In the following methods, a certain set of images are investigated to create a PSF (point spread function) model. The purpose of this model is to contain the majority of the information originating from the star and to subtract it from the original data. This model is created by principal component analysis, which will be explained in section 2.6. The set of images investigated per technique is visualized in figure 3.

2.1 ADI

The first imaging technique that will be discussed is ADI, which stands for angular differential imaging. In this method, a set of images I is acquired with a telescope (in this case the VLT) while the instrument field derotator is turned off. This set of images are taken per wavelength channel at different times, which is visualized in figure 3 by the

green box. A field derotator is a function of the telescope to follow the object and rotate against the rotation of the earth. This rotating option prevents that the field of view (FOV) turns around the central star over the course of an observation. By turning this derotation option off, the potential exoplanet will appear in different locations around the star. The PSF of the star, on the contrary, does not change much when rotated. This is displayed in the first column in figure 1, where the red dot represents an exoplanet and the central region the PSF of the star. The set of images I will then be put together to build a model of the stellar PSF, which is done by principal component analysis and is represented by the second column of figure 1. This analysis seeks a new orthonormal basis to represent the data. The components of this bases represent images called principal components, which are sorted by decreasing variance. By taking the first couple of principal components, a PSF model can be created with barley any data of the exoplanet(s) in it. This is because the planets have the property to have a minimal effect on the variance. This property is enhanced by the fact that the planet appears in different locations around the star. When the whole set of images is considered, the information of the planet will be 'smeared out'. A more detailed explanation is written in section 2.6. After creating this PSF model, this is subtracted from the original images (the first column in figure 1) to create images where the planet should be more visible. These adapted images are represented by the third column in figure 1. Finally by derotating each image, another set of images is created where the planet is on the same location. On figure 1 the rotated images are presented in column 4. Stacking these images by taking the median of this set, results
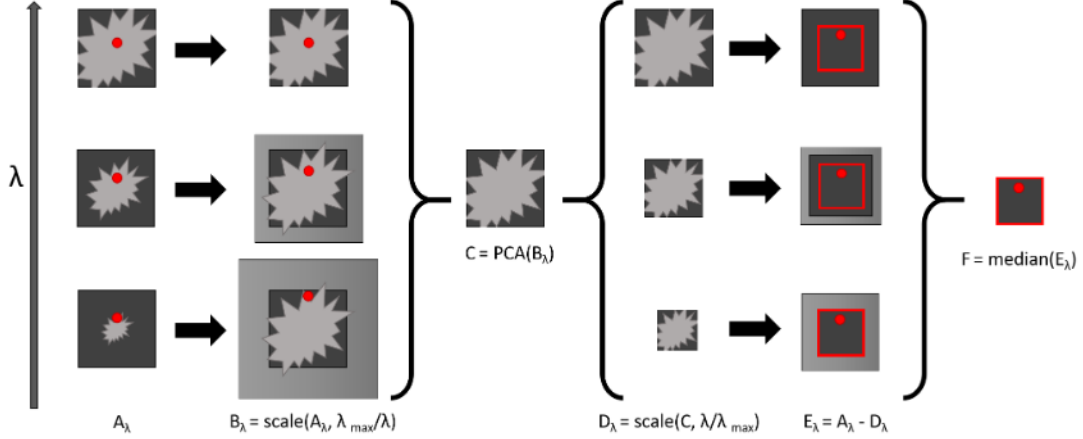
Figure 2: The steps done to perform SDI displayed schematically. First the images are made at different wavelengths, then they get scaled so that their FWHM aligns forming a set B. A PCA gets done on the images of set B. The image formed by the first principal components gets scaled to fit the FWHM of the original images, forming a set D. Each PSF model in set D gets subtracted from each corresponding image in set A, revealing the exoplanet. Finally the median gets taken from these images.

in the final image where the planet should be better visible. This process is done with a set of images of 39 different wavelength channels, so a total of 39 PCAs will be conducted. This corresponds to shifting the green box over all rows in figure 3.

2.2 SDI

SDI (spectral differential imaging) is another imaging technique, which is quite similar to ADI. Instead of considering a set of images at different times in the same wavelength, SDI considers a set of images at different wavelengths at the same time. These set of images are presented in the first column of the schematic overview in figure 2 and by the red box in 3. The red dots on the images represent again the potential planet. This method makes use of the point spread function. When light enters from a distant point source, the light will be diffracted when entering the telescope. However, the PSF is wavelength dependent. It will have the same shape, but the full width at

half maximum will differ. This is described by the Rayleigh criterion:

$$\Delta(\lambda) \propto \frac{\lambda}{D}, \tag{1}$$

with D the diameter of the lens of the telescope. This means that the FWHM of longer wavelengths is bigger. To compare the considered set of images, which are taken in different wavelengths, and to make a good PSF model via a PCA, each image has to be scaled with a scale factor

$$S(\lambda) = \frac{\lambda_{ref}}{\lambda}. \tag{2}$$

Here the reference wavelength is chosen to be the longest wavelength observed. This is done to prevent under-sampling of the residual star light by downscaling the images. This has the consequence that the FWHM's of all images equals the FWHM of the largest wavelength. By performing the change of scale, the place of the potential exoplanet will be shifted. To work with the whole set of images, their size has to be the same. This
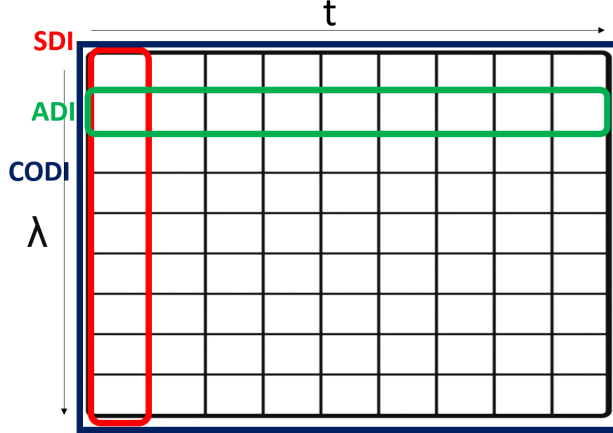
Figure 3: Overview of the different imaging techniques. The big grid represents all images used in the differential imaging techniques (a box represents an image). Every column contains images taken on the same time t, but taken in different wavelength λ. The boxed regions represent the set of images used in the corresponding technique.

will have the consequence that the outside of the scaled images get cut off. This scaling step can be seen in the second column of figure 2. The light grey contours on the scaled images represent the data that has been cut off. Next the PCA is performed on this set of images. Planetary signals are minimal in the first principal components, due to the same reasons as with ADI: the planet should have a minimal influence on the variance. This is again enhanced by the fact that the planet seems to be at different distances from its star. The first principal components form a PSF model of the star without the contribution of its companion(s) , this is represented in column 4 in figure 2. Afterwards, the model is subtracted from the input images. However, the PSF model first has to be scaled back by multiplying it with a factor

$$R(\lambda) = \frac{\lambda}{\lambda_{max}}. \tag{3}$$

This process is represented by the fourth column of figure 2. By scaling the images back there is again a loss of data to match the size

of the other images. Subtracting the model should reveal the exoplanet on each image. Again the final result is formed by stacking the processed images by taking the median , resulting in the final master image. This master image will be smaller than the one obtained by ADI, due to the scaling of the images. This process is done for all different time instances, which corresponds to shifting the green box in figure 3 over all columns.

2.3 CODI

CODI stands for combined differential imaging. Here images in different wavelengths and at different times are considered simultaneously. This is represented by the blue box surrounding all images in figure 3. Note that with CODI the derotation option of the telescope is also turned off. As with SDI each image gets scaled with the scale factor given in equation 2. Now the PCA is performed with all the images to create a PSF model where the planetary signal is minimal. This PSF model gets subtracted from all input images. Finally rotating each image according to their time of

5

capture and rescaling every image back with equation 3, a set of images is created with the possible exoplanet(s) all on the same spot. The median of this set results in a master image of the exoplanet(s).

2.4 ASDI

ASDI (angular and spectral differential imaging) is the combination of where first ADI and then SDI is performed. Note that with ASDI the derotation option of the telescope is turned off. So with ASDI, first a PCA is done for each wavelength on the images taken at different times, just as in ADI. In the light of figure 3, this corresponds to taking a PCA of each row. The first principal components of each row are used to create the PSF model and is subtracted from each set of images. Now SDI is performed on all images taken at the same time instance. The PSF model is created and subtracted from the processed images by ADI. Finally the images are derotated according to their time frame so that the exoplanet aligns on every image. Taking the median of these results in the master image. As a result of SDI, the images are smaller due to the scaling of the images. In the light of figure 3, this method corresponds to shifting the green box over all rows while performing ADI, and afterwards moving the red box over the different columns while executing SDI.

2.5 SADI

SADI (Spectral and Angular Differential Imaging) is exactly the same as ASDI, but here order is switched. First SDI is executed but without stacking the images at the end. Afterwards ADI is performed as described above to create the final image. In the light of figure 3, this method corresponds to shifting the red box over all rows while performing SDI, and afterwards moving the green box over the different columns while executing ADI. The final image of SADI will also be smaller than the input images due to the scaling of SDI.

2.6 PCA

In all differential imaging techniques described above, it was required to get rid of the contribution of the star to make the planet better visible. An image or PSF model was created out of (normalized) data and was afterwards subtracted of this data, as explained in the previous sections. This model was not created by taking a median, but by the use of principal component analysis. The latter seeks to represent observations, like images, in a form that enhances the mutual independence of contributory components. This is done by creating a new set of independent variables of the old variables, by choosing a new coordinate basis. The power of PCA is that, because these new variables are independent of each other, they contain different information of your data. By dropping some of these variables, certain information is filtered out of your data. This property gives the advantage of subtracting certain information, which preferable is that of the star and not from the planet. PCA is a widely known technique which can be applied in other domains, like in statistics, signal processing and elsewhere. Here the application for images processing is focused on and will be explained.

.

PCA has its origin in linear algebra. When multiple images are used, an analogy can be made with a multidimensional vector space where properties of algebra can be applied. To understand this analogy, an image has to be represented by a vector. An image consists of

pixels which each contain a certain value (in our case a flux). This image can be represented by a matrix of shape $M \times N$ (M, $N \in \mathbb{N}$), where each component represents one pixel. By putting each column behind each other, a large vector is created of size $MN \times 1$, which is visualized on figure 4 on the left. This process can be done for multiple images and every vector of size $MN \times 1$ can be put next to each other to create a matrix of size $MN \times K$, where K represents the amount of images.

When $K = 2$ the process of PCA can easily be visualized. In this case a $MN \times 2$ matrix is created where every row represents the values of the same pixel. These values can be plotted in a 2D graph, where every point represents a pixel and the coordinate axes consist out of the values of each pixel in 1 image. PCA then seeks new coordinate bases, and these are chosen along the direction of maximum variance. This process is represented on figure 5, where this direction is represented by the red line. The second direction (green line on figure 5) is then again chosen along maximum variation which is perpendicular on the red line. Now the datapoints can be represented along these new coordinate axes. These axes are called principal components (PC's). In this case, dropping variables means reducing the dimensionality of the graph to 1 dimension. This is done by projecting the data on one of the coordinate axes or PC's. Since the green and red line were perpendicular to each other, they contain different information of your data.
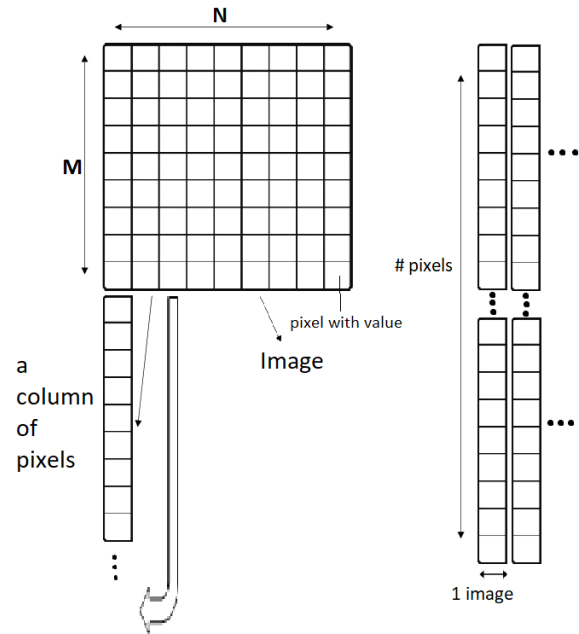

Figure 4: **Left:** Creating a long vector of size $MN \times 1$ out of an image. **Right:** Creating a $MN \times K$ matrix, where K represents the amount of images.

When K is a large number, this process can not be visualized as we can not plot something in more than 3 dimensions. The same process is repeated, but now it is done with linear algebra. When K images of size $M \times N$ are considered, a matrix A can be constructed of size $MN \times K$ with the process represented on figure 4. Of this matrix , the covariance matrix $B = cov(A_T)$ is constructed of size $K \times K$, which is linked with the correlation and variance. Then K eigenvectors of matrix B can be calculated and these are orthonormal to each other since B is symmetric by construction. Now for the analogy with the 2D case: these eigenvectors represent the directions along the variance and their corresponding eigenvalues determine the magnitude of this variance. Going back
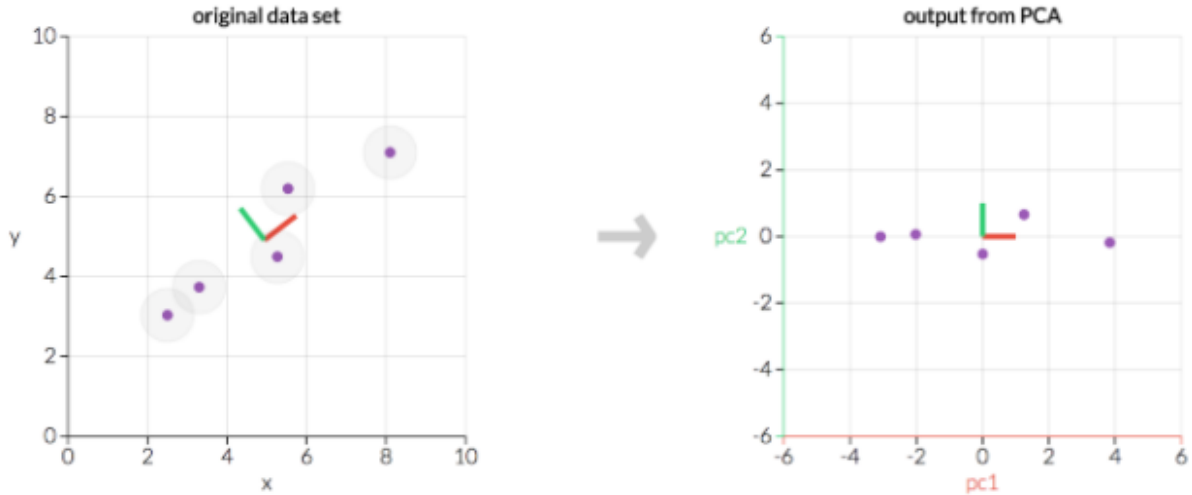
Figure 5: A 2D example where five data points are transformed using PCA [6].

to the multidimensional case, a matrix P can be created where the eigenvectors are the columns. These eigenvectors are sorted according to the magnitude of their eigenvalues (so column 1 is the eigenvector with the biggest eigenvalue). The data contained in matrix A can be represented by these new eigenvectors, resulting in a new matrix $C = AP$. In this new matrix every column is independent of each other since the columns of P are the orthogonal eigenvectors (the independent variables). In this case, the columns of C are the principal components. These columns can be rearranged to an image by doing the procedure in reverse visualized on figure 4.

The PC's with the most 'information' of the star have to be subtracted to create an image with a visible planet. Since the principal components are sorted by decreasing variance, the first PC's contain more information of the star. So by subtracting the first principal components, more light of the central star will be subtracted.

Since the columns of the matrix C represent the principal components, the maximum amount of PC's used in the differential methods is limited to the number K, the amount of images used. This means that the maximum PC's used for SDI equals 39, since SDI splits the data sets into wavelength channels and 39 is the amount of channels in SPHERE. For the reason that ADI splits the datasets into time sets, the amount of PC's equals the amount of time instances per wavelength N_λ^{tot}. For CODI, the amount of principal components equals $39 \times N_\lambda^{tot}$, because it performs 1 PCA for all images. It is chosen that ASDI and SADI will have the same amount of PC's for the SDI and ADI part. This has the consequence that the maximum amount of PC's used is limited to 39. This all is summarized in table 1.

3 Results

3.1 Datasets

The following solar systems were considered: β Pictoris, 51 Eridani and HR8799. The data of the first target was obtained by a newer version

Table 1: The theoretical maximum amount of PC's PC_{max} that can be used in the different differential methods, where N_λ^{tot} stand for the number of time instances per wavelength.

	ADI	SDI	ASDI	SADI	CODI
PC_{max}	N_λ^{tot}	39	39	39	$39 \times N_\lambda^{tot}$

of the processing algorithm. Here the data of every method was given per wavelength, which gave the opportunity to investigate the data in more detail. This means that with the differential methods, the processed input images were eventually derotated and stacked along there wavelength. The amount of PC's used in SADI and ASDI could also be different for the ADI- and SDI-part. The maximum of PC's of both parts equaled 5. This means that per wavelength, 25 different images were created. Unfortunately due to technical problems, the datasets of CODI and SDI were not available for research. For ADI, only 2 PC's were used. This low number was also a result of the technical issues. The data of the two other systems differ from β Pictoris since the data is not categorized by wavelength. Here the average is taken over all wavelengths to create one image per used amount of PC's. This is due to technical problems which prevented the possibility to use the new version of the algorithm. The data used on 51 Eridani and HR8799 is from the research conducted by S. Kiefer et aL. (2021) [3]. However, in these datasets more PC's had been used than with β Pictoris since they used more input images. A summary of the maximum used PC's is given in table 2. Like mentioned before, HR8799 is a solar system with 4 known exoplanets. However, only the planets HR 8799e and HR 8799d are within the field of view of SPHERE. After the scaling done in SDI (see section 2.2 and as seen in figure 6), only the closest planet HR 8799e remains on the data. This means that only

with ADI, the two exoplanets can be detected.

In figure 7, the difference can be seen for β Pictoris between a result of an arbitrary differential method and a result where no imaging technique is used. Here all the input data was just derotated and stacked.

3.2 Signal to noise

In all results, the signal to noise ratio S/N is calculated for gaining a quantity for the quality of the imaged planet. First the exoplanet had to be detected if possible. This was done by implementing the module photutils.detection [1]. This module contained the algorithm DAOFIND [13], which checks for local density maxima that have a peak amplitude greater than a certain threshold value T and have a size and shape similar to a 2D Gaussian. For choosing the threshold value, different methods have been used for getting the better results. In the majority of the data, the median μ and the standard deviation σ of the data was calculated. Then the treshold value was chosen to be $a \cdot \sigma$, where a is a constant. This constant was chosen in that way that the treshold value was under the flux of the planet, which was manually checked. When a value bigger than T was found, a 2D Gaussian was fitted through the PSF with a Full Width Half Maximum (FWHM) of minimal 3 pixels. Any Gaussian with a smaller FWHM will not be detected by this algorithm. This algorithm was applied to a small region around the planet, which was

Table 2: The maximum amount of PC's PC_{max} used in the different differential methods for every system.

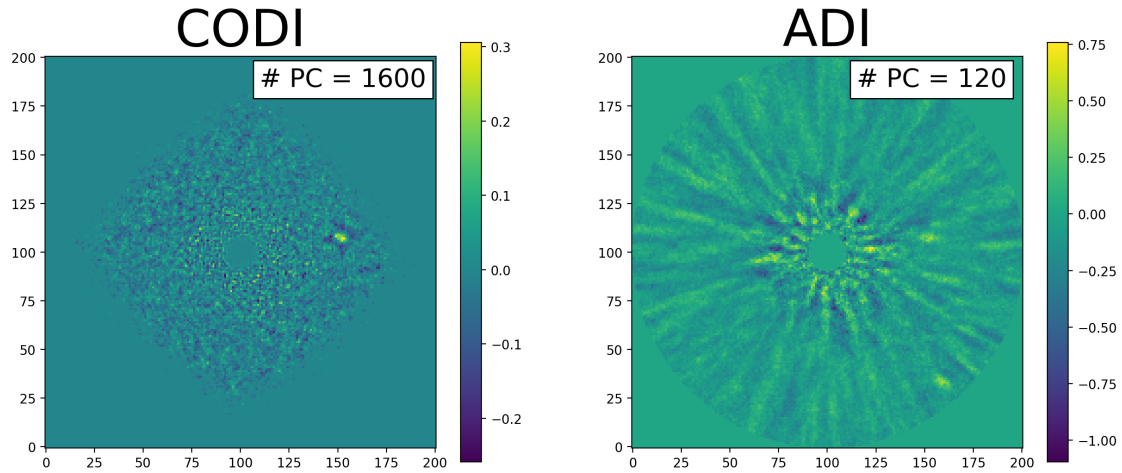| System	ADI	SDI	ASDI	SADI	CODI
β Pictoris	2	/	5	5	/
51 Eridani	90	30	15	15	900
HR8799	180	30	15	15	1800

Figure 6: **Left:** Image of HR8799 created by CODI given with the amount of PC's used. Here the data has been cut due to scaling **Right:** Image of HR8799 created by ADI, where the data was not cut.
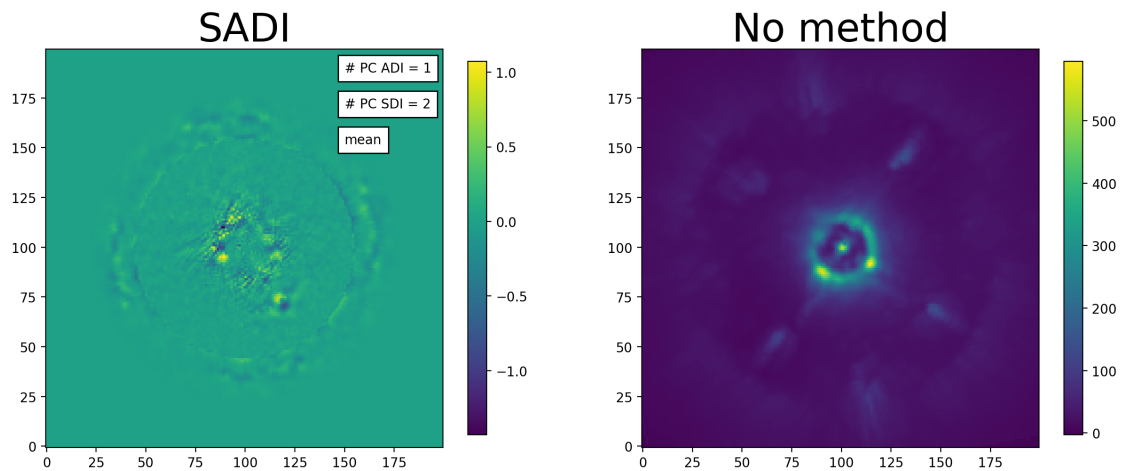
Figure 7: **Left:** Image of β Pictoris created by SADI, where the amount of PC's is given. **Right:** The resulting image of β Pictoris when all input data is derotated and stacked without using any differential method.

10

determined by eye. After the position of the planet was determined, the S/N was calculated with aperture photometry by using the module photutils.aperture in python. This method intends to get a estimation of the magnitude of a source by encircling it and calculating the median value of the pixels in that circle. The radius of the circle was taken at one FWHM of the source. This was done by fitting a 2D Gaussian through the source. The background noise was calculated for a bigger region to create a better estimation. This region was taken at the same radial distance from the center, since the background noise is radially dependent [3]. The background was calculated by taking the root mean square of all the data points in this region, excluding the position where the planet was. The considered regions for calculating the signal and noise is visualized by figure 8. Eventually the median value of the signal and noise were divided.

3.2.1 HR8799d, HR8799e and 51 Eridani b

The results for HR8799d, HR8799e and 51 Eridani b are plotted in figures 19 and 29, which are displayed in the appendix. Each method was applied to the mean image of all the wave lengths.

3.2.2 β Pictoris b

The process above was for β Pictoris b implemented per wavelength, but not for all wavelengths. First the set of all images of per wavelength range M_λ were examined by eye to confirm for the presence of an exoplanet. When no exoplanet was visible in M_λ for all different combinations of PC's, the S/N was not calculated. For the wavelengths where a planet was visible by eye for a certain combiantion of used PC's, a S/N value was calculated for the whole set M_λ. When no planet was detected by the DAOFIND algorithm, the position was chosen to be the median of the of the detected positions of the planet in the same wavelength to get a value for the S/N. The radius of the aperture was then chosen to be the FWHM of a source determined in another image of the same wavelength. It was checked that the FWHM did not change significantly of sources where different PC's were used. For SADI and ASDI, the calculated S/N were put in a 2D array, where the axes determine the amount of used PC's in the ADI and SDI part. This 2D arrays are called PC grids. This resulted in 39 PC grids, one for each wavelength. To compare the pattern of each PC grid in different wavelengths, the values were divided by their maximum value to set the maximum value of the S/N equal to 1 in every wavelength. This way every wavelength is evenly weighted. This was done to get an overview for which PC's the differential technique was best and not for the quality of the images in a certain wavelength. After this normalization, the median was taken of all PC grids, which resulted in figure 11 and 9 for respectively SADI and ASDI. The standard deviation of every pixel was calculated using the median values of figure to get an understanding for a possible pattern . This is plotted in figures 10 and 12.

For ADI, only two PC's were available. Here all S/N values could be plotted in a 2D array for every wavelength(see figure 14). The maximum values for each wavelength can be seen in figure 13. When no planet was found in a wavelength, the S/N value was set to zero.
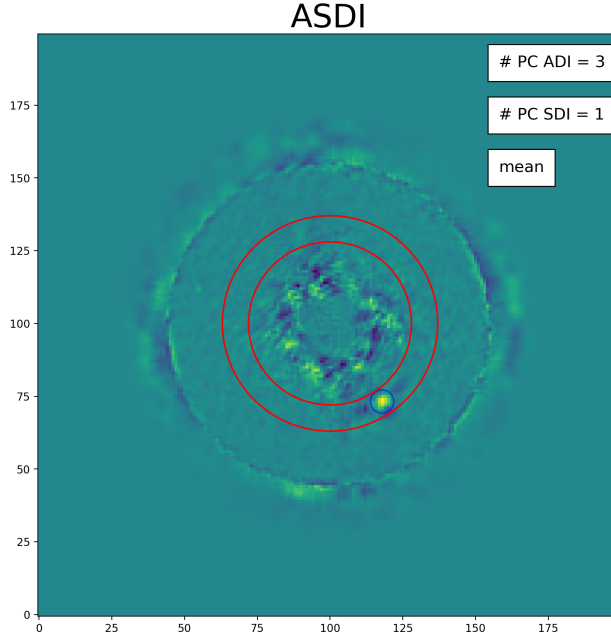
Figure 8: One example where the regions are marked for the calculation of S/N. The blue circle represents the aperture around the source (the radius here is enlarged for visual purpose) and the red region without the aperture was considered for calculating the background level,excluding the blue circle.
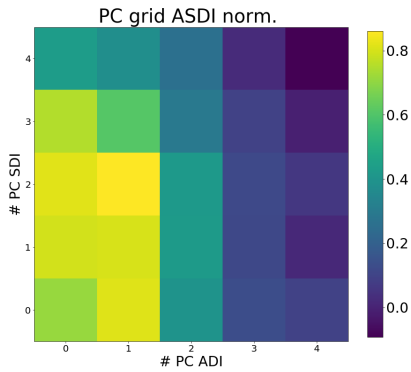

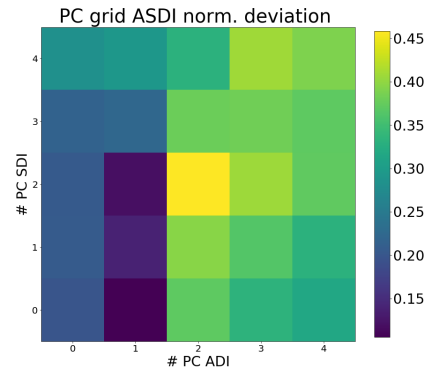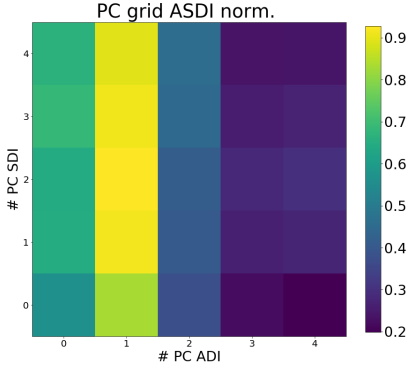Figure 9: The median of the 39 normalized PC grids of ASDI.

Figure 10: The standard deviation of the 39 normalized PC grids of ASDI.

Table 3: The measured distance between the planet and its parental star.

pixel distance	ADI	CODI	ASDI	SADI
HR8799e	53.0	51.8	/	/
HR8799d	88.7	/	/	/
51 Eridani b	59.4	59.4	59.3	59.1

Figure 11: The median of the 39 normalized PC grids of SADI.
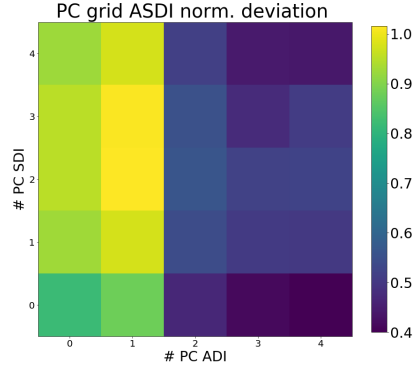
Figure 12: The standard deviation of the 39 normalized PC grids of SADI.
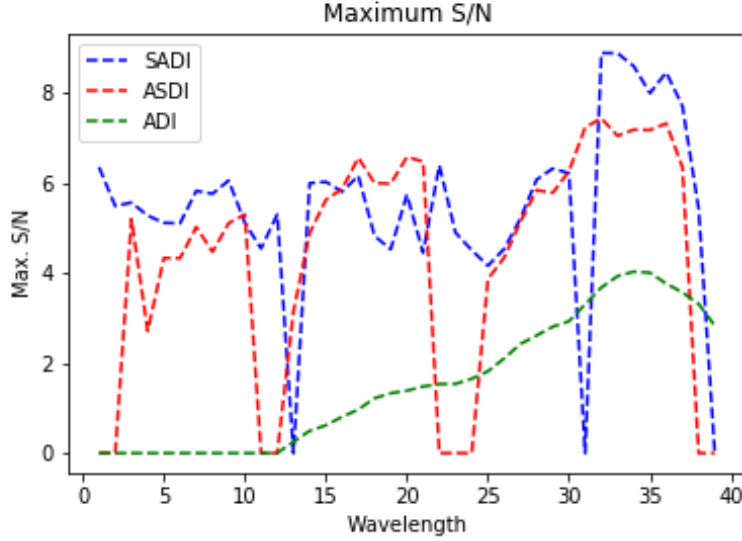

Figure 13: The maximum S/N of the 39 wavelengths of ADI, SADI and ASDI.

Table 4: The Calculated orbital radii, velocities and periods of the exoplanet HR8799e in the imaging techniques ADI and CODI. With the values found in other literature as a comparison.* This is the value of the Semi-Major Axis.

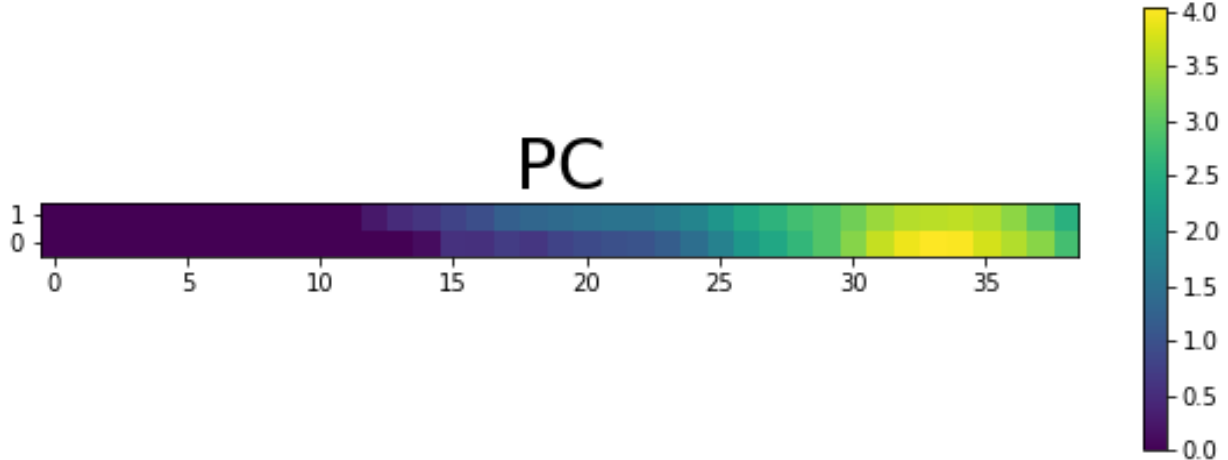| HR8799e	ADI		CODI		Literature
	R_{max}	$R_{measured}$	R_{max}	$R_{measured}$	
Orbital Radius [AU]	$18.0^{+0.3}_{-0.3}$	$16.3^{+0.3}_{-0.3}$	$17.6^{+0.3}_{-0.3}$	$15.9^{+0.3}_{-0.3}$	$16.4^{+2.1}_{-1.1}*$ [4]
Orbital Velocity [km/s]	$8.0^{+0.4}_{-0.4}$	$8.8^{+0.4}_{-0.4}$	$8.1^{+0.4}_{-0.4}$	$8.9^{+0.4}_{-0.4}$	
Orbital Period [year]	64^{+2}_{-2}	55^{+2}_{-2}	62^{+2}_{-2}	53^{+2}_{-2}	~ 50[8]

13

Figure 14: The S/N of the 39 wavelengths of ADI. The vertical axis represent the amount of PC's used, the horizontal axis represent the wavelength.

Table 5: The Calculated orbital radii, velocities and periods of the exoplanet HR8799d in the imaging technique ADI. With the values found in other literature as a comparison.* This is the value of the Semi-Major Axis.

HR8799d	ADI		Literature
	R_{max}	$R_{measured}$	
Orbital Radius $[AU]$	$30.9^{+0.3}_{-0.3}$	$27.3^{+0.3}_{-0.3}$	27.0^* [12]
Orbital Velocity $[km/s]$	$6.0^{+0.2}_{-0.2}$	$6.8^{+0.2}_{-0.2}$	
Orbital Period $[year]$	144^{+4}_{-4}	119^{+3}_{-3}	115.9 [12]

Table 6: The Calculated orbital radii, velocities and periods of the exoplanet 51 Eridani b in the imaging techniques ADI and CODI. With the values found in other literature as a comparison.* This is the value of the Semi-Major Axis.

51 Eridani b	ADI		CODI		Literature
	R_{max}	$R_{measured}$	R_{max}	$R_{measured}$	
Orbital Radius $[AU]$	$18.1^{+0.3}_{-0.3}$	$13.0^{+0.3}_{-0.3}$	$18.1^{+0.3}_{-0.3}$	$13.0^{+0.3}_{-0.3}$	$11.1^{+4.2}_{-1.3}$*[10]
Orbital Velocity $[km/s]$	$7.9^{+0.4}_{-0.4}$	$10.9^{+0.5}_{-0.5}$	$7.9^{+0.4}_{-0.4}$	$10.9^{+0.5}_{-0.5}$	
Orbital Period $[year]$	$58.2^{+1.3}_{-1.3}$	$35.5^{+1.2}_{-1.2}$	$58.2^{+1.3}_{-1.3}$	$35.5^{+1.2}_{-1.2}$	$28.1^{+17.2}_{-4.9}$[10]

Table 7: The Calculated orbital radii, velocities and periods of the exoplanet 51 Eridani b in the imaging techniques ASDI and SADI. With the values found in other literature as a comparison.* This is the value of the Semi-Major Axis.

51 Eridani b	ASDI		SADI		Literature
	R_{max}	$R_{measured}$	R_{max}	$R_{measured}$	
Orbital Radius $[AU]$	$18.1^{+0.3}_{-0.3}$	$13.0^{+0.3}_{-0.3}$	$18.0^{+0.3}_{-0.3}$	$12.9^{+0.3}_{-0.3}$	$11.1^{+4.2}_{1.3}$*[10]
Orbital Velocity $[km/s]$	$7.9^{+0.4}_{-0.4}$	$10.9^{+0.5}_{-0.5}$	$7.9^{+0.4}_{-0.4}$	$10.9^{+0.5}_{-0.5}$	
Orbital Period $[year]$	$58.0^{+1.3}_{-1.3}$	$35.4^{+1.2}_{-1.2}$	$57.8^{+1.3}_{-1.3}$	$35.3^{+1.2}_{-1.2}$	$28.1^{+17.2}_{-4.9}$[10]

3.3 Orbit

With the detected postions of the planets, information about the orbit of the exoplanet could be determined. The system β Pictoris is not mentioned in this section, since the inclination angle of the system is $i = 89.01^{+0.01}_{-0.01}{}^\circ$ [5]. More information about the inclination angle can be found in the discussion (see section 4.2). To calculate the data in the following subsection only the results of ADI, CODI, ASDI and SADI were used for 51 Eridani b, ADI and CODI for HR8799e and only ADI for HR8799d, because they were for each exoplanet the only methods where a visible/usable image of the exoplanet were formed. For each planet and each imaging method the average radius of the orbit has been calculated twice. Once assuming the measured radius is the effective radius and once assuming the measured radius is the smallest possible radius that can be measured from earth. A more deeper explanation about this can be found in the discussion section. By calculating these two radii per planet an interval is created, where the exoplanet has to lie in.

3.3.1 Radius

The orbital radii of the exoplanets have been calculated with the detected positions. The center of the image was used for the location of the parent star. Both the location of the exoplanets and their stars were given in pixels. In the data, it was found that the $\frac{arcsec}{pixel}$ ratio was $0.00746 \frac{arcsec}{pixel}$ for the images of the HR8799 and the 51 Eridani systems. The orbital radii were then calculated with the following formulae:

$$R_{min} = d_p \cdot r \frac{2\pi}{360 \cdot 60 \cdot 60} \cdot D_{star} \qquad (4)$$

$$R_{max} = d_p \cdot r \frac{2\pi}{360 \cdot 60 \cdot 60} \cdot D_{star} \cdot \frac{1}{\cos(i)}, \quad (5)$$

where d_p is the measured distance of the star to the exoplanet in pixels, $\frac{2\pi}{360 \cdot 60 \cdot 60}$ the factor that makes the conversion from arcseconds to radians, r the arcsec-pixel ratio, D_{star} the distance between earth and the parental star in astronomical units and i the inclination angle of the plane of the planet's orbit with the line of sight of the observer. These values can be found in table 8, where one parsec equals 206264 astronomical units. The results found for the orbital radii are displayed in table 4 for HR8799e, in table 5 for HR8799d and in tables 6 and 7 for 51 Eridani b.

3.3.2 Period

The periods of the exoplanets were calculated with Kepler's third law:

$$T^2 = \frac{a^3}{M}, \qquad (6)$$

where a is the the orbital radius in AU and M the mass of the parental star in $M_\odot$ (see table 9). The period of the orbit T is then given in years. The results found for the orbital periods are displayed in table 4 for HR8799e, in table 5 for HR8799d and in tables 6 and 7 for 51 Eridani b.

3.3.3 Orbital Velocity

Calculating the velocities at which the exoplanets orbit their parental stars wasn't a challenge either. For this the length of the orbit had to be calculated and then divided by the period of the orbit as follows:

$$v_{orbit} = \frac{2\pi R_{AU}}{T} \qquad (7)$$

Table 8: The values of D_{star} in parsec pc and the inclination angele i in degrees, given with their source.

Exoplanet	Distance D_{star} $[pc]$	angle i $[°]$
51 Eridani b	$29.7823^{+0.12}_{-0.12}$ [9]	136^{+10}_{-11} [10]
HR8799 d	$41.2925^{+0.1502}_{-0.1502}$ [9]	28.0 [12]
HR8799 e	$41.2925^{+0.1502}_{-0.1502}$ [9]	$25.0^{+8.0}_{-8.0}$ [4]

Table 9: The values of the parental stars in solar masses $M_\odot$, given with their source.

System	Mass star M $[M_\odot]$
51 Eridani	$1.75^{+0.05}_{0.05}$ [7]
HR8799	$1.47^{+0.12}_{0.17}$ [11]

This gives the orbit in astronomical units per year. To convert it to $\frac{km}{s}$, it must to be multiplied with the factor $\frac{1.49 \cdot 10^8 \frac{km}{AU}}{365 \cdot 24 \cdot 3600 \frac{s}{year}}$. The results found for the orbital velocities are displayed in table 4 for HR8799e, in table 5 for HR8799d and in tables 6 and 7 for 51 Eridani b.

4 Discussion

Before discussing the results in detail, it can be seen that the differential methods have a large effect on the input data on figure 7.

4.1 Signal to Noise

4.1.1 HR8799 and 51 Eridani

For the HR8799 and 51 Eridani planetary systems the signal to noise ratio has roughly the same results: a higher ratio than 1 in CODI, ADI, SADI and ASDI and a lower ratio than 1 in SDI. This means that the flux of the noise outweighs the flux originating from the planet in SDI and the other way around with the other techniques. In the HR8799 system there is a clear difference between the S/N of HR8799e and HR8799d. This is due to the difference in the radius of the orbits of the two planets. HR8799e is closer to their parental

star and so suffers more from light pollution of the star making it more difficult to see. It is also noticable that in the HR8799 images the S/N for SADI and ASDI is higher then the S/N of ADI. When looking subjectively to the images by eye, HR8799e is much more visible in ADI then when looking at the ASDI and SADI systems. The explanation is found when looking separately to the flux coming from the planets and coming from the noise for the different imaging techniques. The flux originating from the planet is greater in ADI, but so is the flux originating from the noise.

4.1.2 β Pictoris

For the PC grids, it is noticable that there is a pattern in the PC grids for ASDI. The high values in figure 9 and the low values in figure 10 in the left region demonstrate that the use of these amount of PC's give good results in all wavelengths. This is different for SADI. High values are found in the left region (see figure 11), but the standard deviation is bigger (see figure 12). This means that the results differed per wavelength channel and no consistent pattern was created. For the data of ADI, it can be concluded that using 1 PC gives better results than using 2. It is also obvious that the detection was better for the

bigger wavelengths.

It must also be noted that there is a possibilty that false sources were detected. For some PC's a negative source is found on the region where the planet was mostly found. This happens when the planet is bright in some wavelengths but dark in others. If the planet shows up partially in the PCA it will be removed with equal strength from all wavelength images. In the ones with no planet signal, the reduction becomes negative. This is demonstrated by an obvious example in figure 15. The positive sources next to it are reduction artifacts, but are considered as planets by DAOFIND. This means that in some cases, the S/N ratio is calculated for false sources.

In figure 13, it can be seen that for bigger wavelengths, all methods gave better results, where SADI gave the highest S/N value. This indicates that the planet radiates more in this wavelength range. It can also be seen that with ADI, the planet is detected in less wavelengths and give lower S/N values.

4.2   Orbit

The Orbital radii of the planets were calculated from images taken at practically the same time. This could lead to the possibility that the measured radius of the planet's orbit is much smaller than the actual orbital radius. To what extent this effect happens depends on the inclination angle of the planet's orbit. The inclination angle is the angle between the plane, wherein the planet orbits, with the line of sight of the observer. The orbit of the planet gets, from a 3 dimensional orbit, projected on a 2 dimensional image. The measured radius of the orbit is therefore oscillating . When the inclination angle, i, is around 90° the plane of the planet's orbit is (almost)

parallel to the line of sight of the telescope. This is why the orbital radius of β pictoris b was not calculated. The inclination angle of the orbit is $i = 89.01^{+0.01}_{-0.01}$ [5] making the $R_{max} \approx 60 \cdot R_{measured}$ (calculated with equation 8), in other words not an ideal system to calculate. When images from only one observation time are used, it might be that the measured radius could be a lot smaller than the actual radius. With an emphasis on 'could', because by chance it might be possible that the measured radius of the planet's orbit is the same as the actual radius of the orbit. This can best be understood when you take a look at the figures 16 and 17. When observations spread over a long time period are made the actual radius of the system can be calculated. If the inclination angle, i, is small, or if the inclination angel is around 180°, the measured distance between the star and the exoplanet is very close to the actual distance between them. This is visualized in figure 18. The correction applied to the measured orbital radius to find the upper limit for the real radius is

$$R_{max} = R_{measured} \cdot \frac{1}{\cos(i)} \qquad (8)$$

with i the inclination angle. There is no way of knowing if you are dealing with this situation or with the one
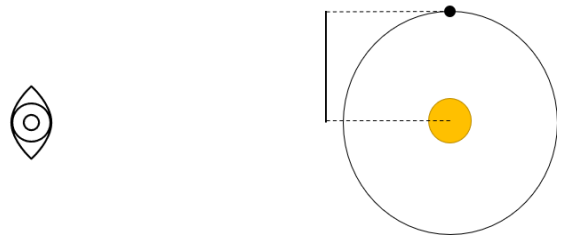

Figure 16: This picture represents a schematical presentation of a planet's orbit with a inclination angle of 90° with the observer's line of sight. Here the measured radius of the orbit is fortuitous the same as the actual orbit of the planet.
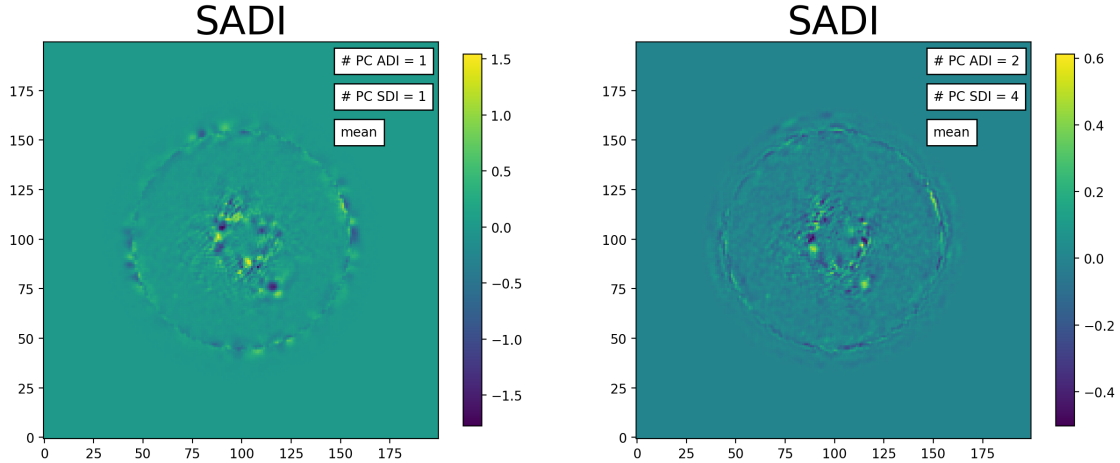
Figure 15: Data of SADI, where the used PC's are given. On the left figure, a negative source is visible next to a positive source. On the right figure only a positive source is observed.
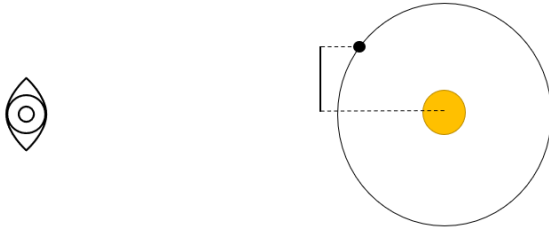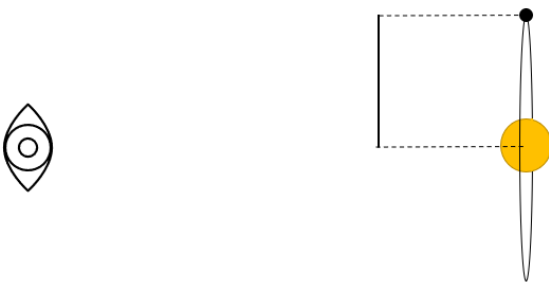

Figure 17: This picture represents a schematical presentation of a planet's orbit with a inclination angle of 90° with the observer's line of sight. Here the measured radius of the orbit is not the same as the actual orbit of the planet.

Figure 18: This picture represents a schematical presentation of a planet's orbit with a inclination angle of (as good as) 0° with the observer's line of sight. Here the measured radius of the orbit is (approximately) the actual orbit of the planet.

5 Conclusion

For HR8799 and 51 Eridani, it can be concluded that the combination of ADI and SDI gave better results than ADI and SDI themselves, according to their signal to noise values. This agrees with our expectations from section 1. It is also noteworthy that the SN-ratio results for SDI on it's own are a lot smaller than the results for ADI on it's own.

For β Pictoris, it can be concluded that the combination of ADI and SDI gave better results than ADI itself. The results are also clearly wavelength dependent, since for bigger wavelengths, higher values are determinend. This is a property of the planet itself and not of the methods itself. The planets radiates more light in this wavelength range. For ASDI it can be concluded that for this system, it is best to use less than 3 PC's for the ADI part and less than 4 for SDI for every wavelength. The best result was obtained with 2 PC's for the ADI part and 3 PC's for the SDI part. For SADI, no conclusion can be made for all wavelengths in the range of SPHERE, since the high values from figure 11 correspond with high values of 12. The best S/N value is calculated with

different amount of PC's in the majority of wavelengths. For ADI, it gave overall better results when using 1 PC instead of two.

The measured radii of the orbits fall well between the lengths and errors of the values found in literature, as displayed in tables 4 to 7. Making it a good conclusion that the radii of the orbits can be calculated out of the data images the way it was done in this paper.

6   Outlook

Due to a lot of technical issues, the images of the systems could not be as good examined as expected. The results came in only 2 weeks before the deadline of this report and did not meet our expectations. Only data of one system could be analyzed with few PC's and not all differential methods. If there was more time to dig in this project, a better and more detailed examination could be done in this project.

On one hand, all methods would be applied with more input images for every system. This would result in a better PCA where more PC's could be created. This would result in a more detailed PC grid. These PC grids would be compared between the different methods, but also between the different systems. The quality of the different differential methods could be better examined and compared with each other. The new algorithm also has the possibility to do this per wavelength range. This would be done for more systems. On the other hand, the goal was to analyze systems where no exoplanet has been imaged yet. This would result in a different (non-biased) approach to analyze the systems.

7   Acknowledgemnts

References

[1] Larry Bradley, Brigitta Sipőcz, Thomas Robitaille, Erik Tollerud, Zè Vinícius, Christoph Deil, Kyle Barbary, Tom J Wilson, Ivo Busko, Hans Moritz Günther, Mihai Cara, Simon Conseil, Azalee Bostroem, Michael Droettboom, E. M. Bray, Lars Andersen Bratholm, P. L. Lim, Geert Barentsen, Matt Craig, Sergio Pascual, Gabriel Perren, Johnny Greco, Axel Donath, Miguel de Val-Borro, Wolfgang Kerzendorf, Yoonsoo P. Bach, Benjamin Alan Weaver, Francesco D'Eugenio, Harrison Souchereau, and Leonardo Ferreira. astropy/photutils: 1.0.0, September 2020.

[2] exoplanet Team. Catalog exoplanet, 2021. [Online; accessed 8-December-2021].

[3] S. Kiefer, A. J. Bohn, S. P. Quanz, M. Kenworthy, and T. SVENS. Kiefer Stolker. Spectral and angular differential imaging with SPHERE/IFS. Assessing the performance of various PCA-based approaches to PSF subtraction. , 652:A33, August 2021.

[4] S. Lacour, M. Nowak, J. Wang, O. Pfuhl, F. Eisenhauer, R. Abuter, A. Amorim, N. Anugu, M. Benisty, and et al. First direct detection of an exoplanet by optical interferometry. *Astronomy Astrophysics*, 623:L11, Mar 2019.

[5] S. Lacour, J. J. Wang, L. Rodet, M. Nowak, J. Shangguan, H. Beust, A.-M. Lagrange, R. Abuter, A. Amorim, R. Asensio-Torres, and et al. The mass of pictoris c from pictoris b orbital motion. *Astronomy Astrophysics*, 654:L2, Oct 2021.

[6] M. Bremms. A one-stop shop for principal component analysis, towards data science [internet], 2017. [Online; accessed 5-December-2021].

[7] B. Macintosh, J. R. Graham, and Barman et al. Discovery and spectroscopy of the young jovian planet 51 Eri b with the Gemini Planet Imager. *Science*, 350(6256):64–67, October 2015.

[8] Christian Marois, B. Zuckerman, Quinn M. Konopacky, Bruce Macintosh, and Travis Barman. Images of a fourth planet orbiting hr 8799. *Nature*, 468(7327):1080–1083, Dec 2010.

[9] Joseph H. Rhee, Inseok Song, B. Zuckerman, and Michael McElwain. Characterization of Dusty Debris Disks: The IRAS and Hipparcos Catalogs. , 660(2):1556–1571, May 2007.

[10] Robert J. De Rosa, Eric L. Nielsen, Jason J. Wang, S. Mark Ammons, Gaspard Duchêne, Bruce Macintosh, Julien Rameau, Vanessa P. Bailey, Travis Barman, Joanna Bulger, and et al. An updated visual orbit of the directly imaged exoplanet 51 eridani b and prospects for a dynamical mass measurement with gaia. *The Astronomical Journal*, 159(1):1, Dec 2019.

[11] Aldo G. Sepulveda and Brendan P. Bowler. Dynamical mass of the exoplanet host star hr 8799, 2021.

[12] Rémi Soummer, J. Brendan Hagan, Laurent Pueyo, Adrien Thormann, Abhijith Rajan, and Christian Marois. ORBITAL MOTION OF HR 8799 b, c, d USINGHUBBLE SPACE

TELESCOPEDATA FROM 1998: CONSTRAINTS ON INCLINATION, ECCENTRICITY, AND STABILITY. *The Astrophysical Journal*, 741(1):55, oct 2011.

[13] Peter B. Stetson. DAOPHOT: A Computer Program for Crowded-Field Stellar Photometry. , 99:191, March 1987.
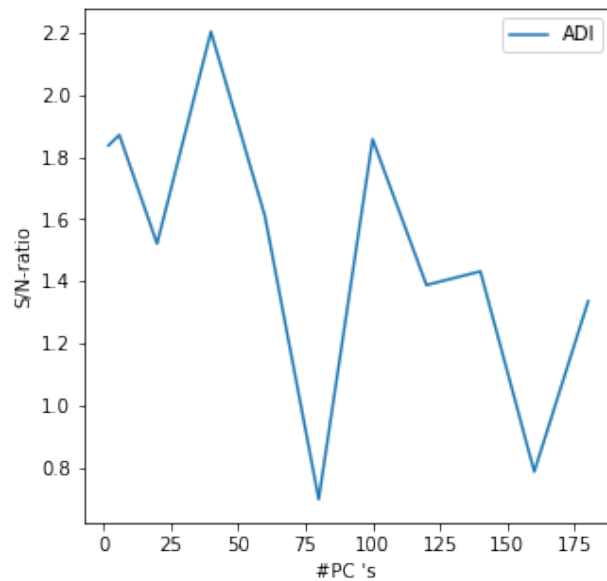
A Appendix

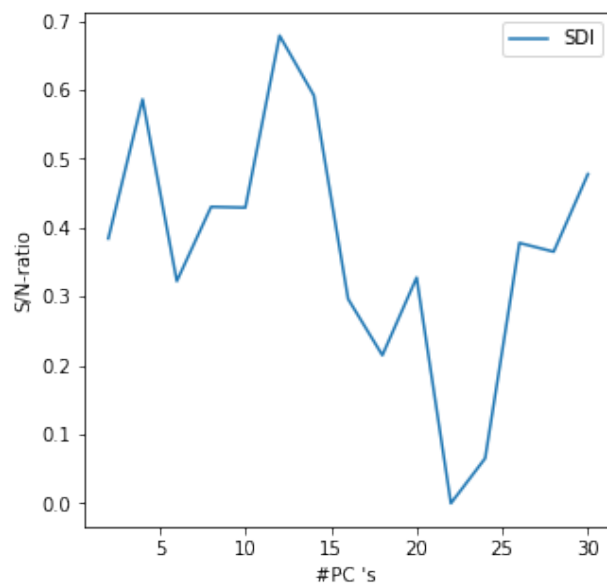Figure 19: The S/N ratios of HR8799e of the ADI method, plotted against the number of PC's.

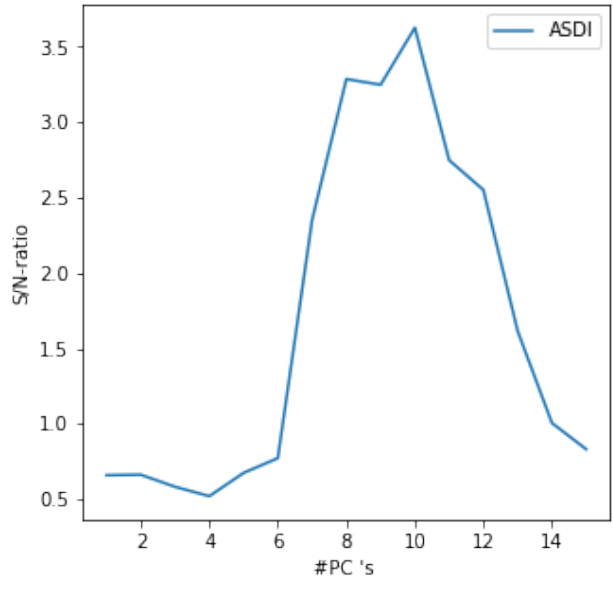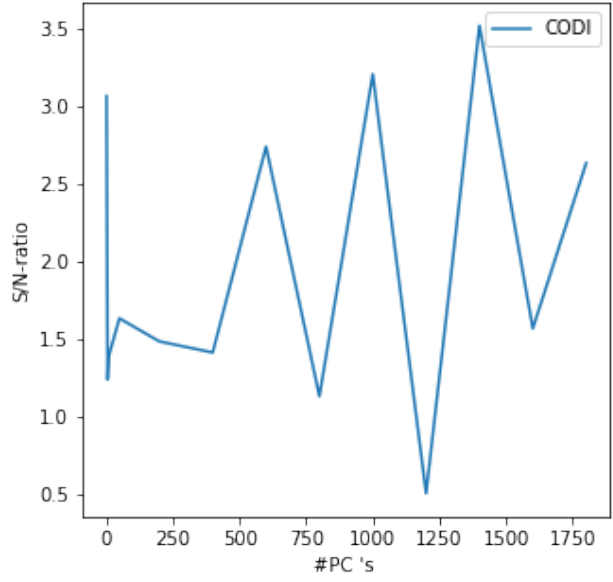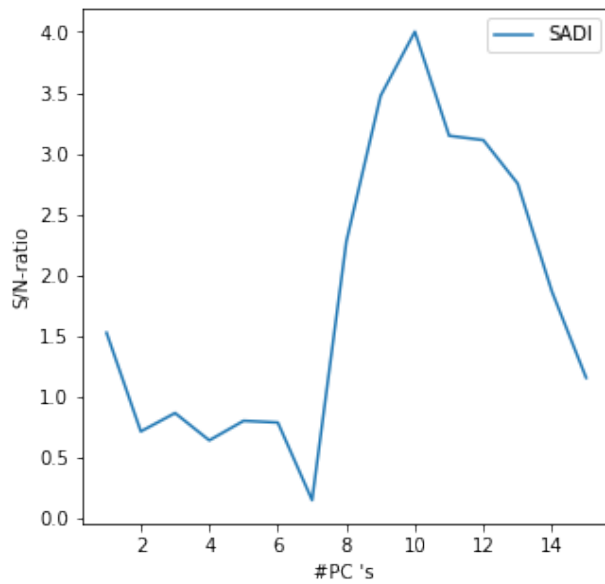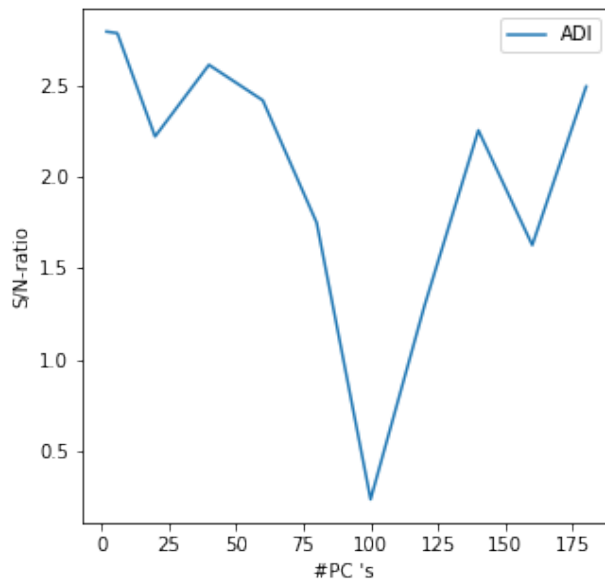Figure 20: The S/N ratios of HR8799e of the SDI method, plotted against the number of PC's.

Figure 22: The S/N ratios of HR8799e of the ASDI method, plotted against the number of PC's.
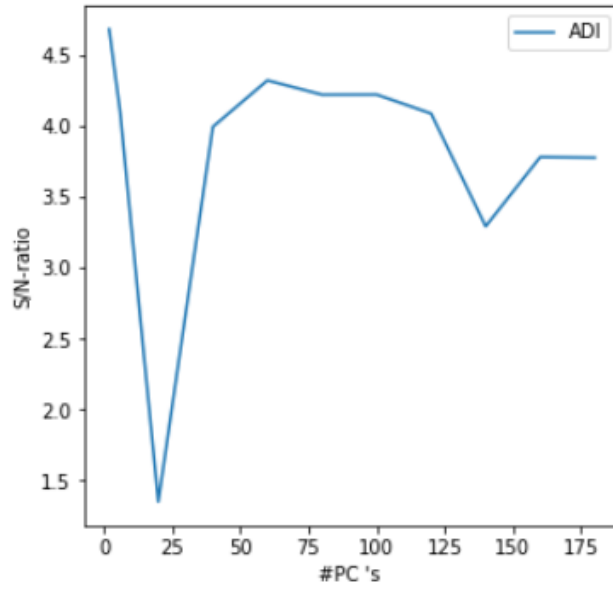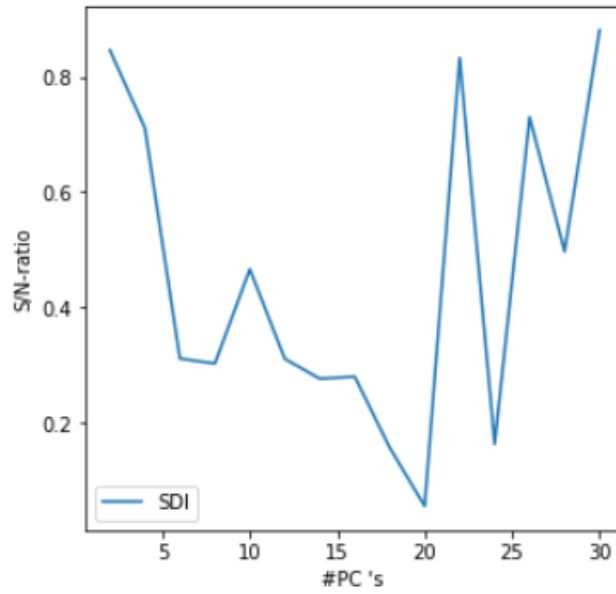

Figure 21: The S/N ratios of HR8799e of the CODI method, plotted against the number of PC's.

Figure 23: The S/N ratios of HR8799e of the SADI method, plotted against the number of PC's.

Figure 24: The S/N ratios of HR8799d of the ADI method, plotted against the number of PC's.

Figure 25: The S/N ratios of 51 Eridani of the ADI method, plotted against the number of PC's.

Figure 26: The S/N ratios of 51 Eridani of the SDI method, plotted against the number of PC's.
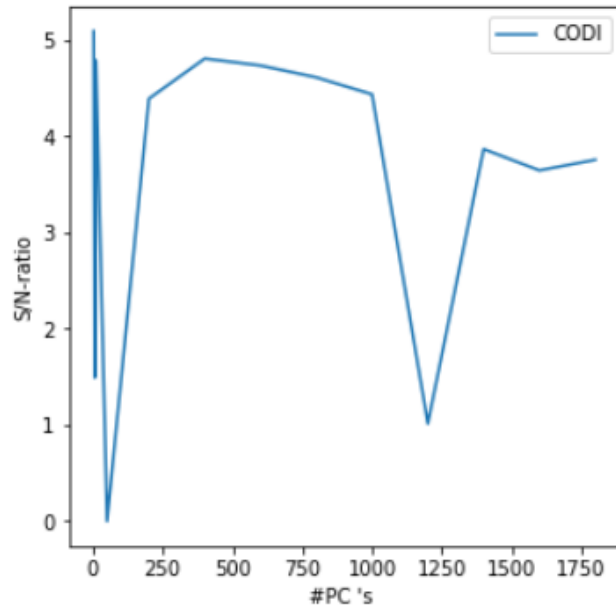
Figure 27: The S/N ratios of 51 Eridani of the CODI method, plotted against the number of PC's.
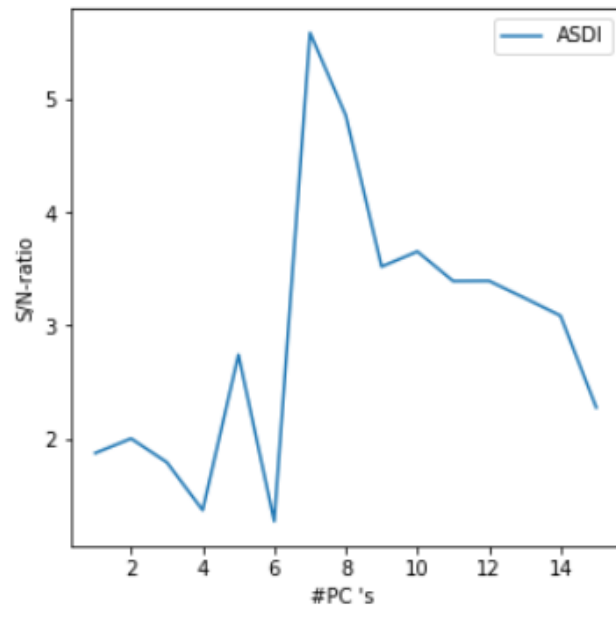

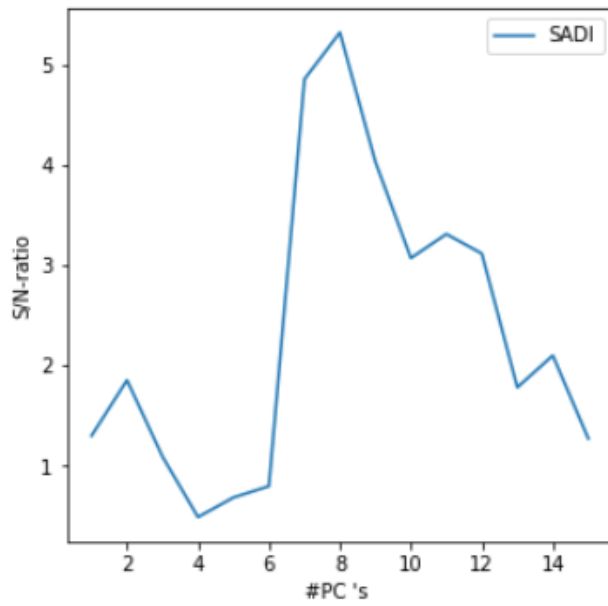Figure 28: The S/N ratios of 51 Eridani of the ASDI method, plotted against the number of PC's.

Figure 29: The S/N ratios of 51 Eridani of the SADI method, plotted against the number of PC's.